High-resolution multicomponent distributed acoustic sensing

Ivan Lim Chen Ning & Paul Sava
Center for Wave Phenomena, Colorado School of Mines

ABSTRACT

Distributed acoustic sensing (DAS) uses an optical fiber together with an interrogator unit to perform strain measurements. The usage of DAS in geophysics is attractive due to its dense spatial sampling and low operation cost if the optical fiber is freely accessible. In the borehole environment, optical fibers for DAS are often readily available as a part of other sensing tools, such as for temperature and pressure. Although the DAS system promises great potential for reservoir monitoring and surface seismic acquisition, the single axial strain measurement of DAS along the fiber is inadequate to fully characterize the different wave modes, thus making reservoir characterization challenging. We propose an acquisition system using five equally spaced helical optical fibers and a straight optical fiber to obtain six different strain projections. This system allows us to reconstruct all components of the 3D strain tensor at any location along the fiber. Analyzing the condition number associated with the geometry of the optical fiber, we can systematically search for the optimum design parameters for our configuration. Numerical examples demonstrate the effectiveness of our proposed method to successful reconstruction of the full strain tensor from elastic wavefields of arbitrary complexity.

Key words: seismic acquisition, borehole geophysics, distributed acoustic sensing, multicomponent, tensor

1 INTRODUCTION

Distributed Acoustic Sensing (DAS) systems use an optical fiber as a distributed array of strain measuring tool. A typical DAS system employs an interrogator unit to send laser pulses into an optical fiber and detect back-scattered light along the fiber. DAS systems that operate on Coherent Optical Time-Domain Reflectometry (COTDR) provide average axial strain measurement through analyzing the perturbed phase difference between back-scattered light along the optical fiber from two points separated by a distance known as gauge length. Acceptable signal-to-noise ratio (SNR) measurements can be achieved using conventional DAS systems that require a gauge length of around 1 m. However, Farhadiroushan et al. (2016) show that the gauge length can be reduced to 5 cm, while maintaining satisfactory SNR using specially designed optical fibers.

Despite the recent technological advances in DAS, multicomponent DAS remains a missing piece of the puzzle to capture the full character of the seismic wavefield. In borehole application specifically, the usage of DAS focuses mainly on reservoir imaging (Mestayer et al., 2011; Mateeva et al., 2012, 2013; Wu et al., 2015; Zhan et al., 2015; Jiang et al., 2016) and velocity model updates (Wu et al., 2015; Li et al., 2015). Although, many examples show that DAS has the potential to provide low-cost reservoir monitoring (Hornman et al., 2015; Dou et al., 2016; Chalenski et al., 2016), the conventional single component DAS measurements makes reservoir characterization challenging. Since DAS acquires strain along the optical fiber, the measurement is a projection of the surrounding strain tensor as a function of the optical fiber position. As indicated by Lumens (2014) and Bakku (2015), the DAS system suffers from broadside sensitivity where the optical fiber is less sensitive to transversally impinging signals.

Although DAS measures axial strain, it is possible to obtain multicomponent data by reconstructing the entire strain tensor using multiple strain projections; manipulating the geometry of the optical fiber allows us to obtain various directions on which to project the strain field. Lim and Sava (2016) provide a basic workflow for recovering multicomponent DAS data using strain projections acquired with dual optical fibers or with a single chirping (variable pitch angle) helical optical fiber. The pitch angle is the complement of the angle between the tangent vector and the axial direction of the DAS cable. The dual optical fibers configuration deploys two helical optical fiber of different constant pitch angle. This configuration is

necessary to obtain sufficient projections for the strain tensor reconstruction. Similarly, Lim and Sava (2016) demonstrate the possibility of full strain tensor reconstruction using one optical fiber with a chirping helix geometry, which provides a broad range of strain projections, albeit at the expense of a complex design. The underlying principle of their method of strain tensor reconstruction is to group consecutive strain measurements along optical fiber(s) within a defined window larger than a gauge length. Despite successfully reconstructing the entire strain tensor, the drawback of this method is the assumption that the seismic wavelength is significantly larger than the defined analysis window. This assumption leads to a strain tensor which is assumed to be invariant within the window. Therefore, the method proposed by Lim and Sava (2016) could not be easily used for acquisition of short seismic wavelengths such as microseismic.

To overcome the limitation of the workflow introduced by Lim and Sava (2016), we propose a configuration with five equally spaced constant pitch angle helical optical fibers and a straight optical fiber. Although we use an increased number of optical fibers, we can obtain six different strain projections at every location and avoid the need to group consecutive strain measurements at different location along optical fiber(s) to get sufficient strain projections for the reconstruction. We thus obtain six different strain projections at every location and reconstruct the full strain tensor without the need to assume invariance in a wide window. The configuration reduces the engineering complexity required to build a multi-fiber cable, and also allows us to systematically analyze the effect of the associated design parameters (gauge length, diameter and pitch angle of the helical optical fibers) on the strain tensor reconstruction. We capture the gauge length in the reconstruction process, which allows us to remove its averaging effect and reconstruct strain data similar to multicomponent geophone point measurements. We note, however, that our method provides the entire strain tensor, in contrast to geophone measurements which provide the displacement vector.

We demonstrate a systematic way to choose the helical optical fiber design parameters (diameter and pitch angle) and the gauge length characterizing our system by analyzing the condition number associated with the geometry our configuration. Using the chosen parameters, we show the reconstruction of the full strain tensor through 3D synthetic examples of arbitrarily complex seismic wavefields.

2 THEORY

The axial strain acquired by DAS captures different projections of the surrounding strain tensor as a function of the location and geometry of the optical fiber. We use the intrinsic coordinate system of a curve as described by Pisano (1988) to express the local coordinate system of the optical fiber with respect to a global coordinate system. We use the tangent vector along the optical fiber to relate the axial strain measurement with the surrounding strain tensor. The relationship between the axial strain and the surrounding strain tensor is given through the coordinate transformation relationship (Young and Budynas, 2002)

$$\bar{\boldsymbol{\varepsilon}} = \mathbf{R}\boldsymbol{\varepsilon}\mathbf{R}^T \ , \tag{1}$$

where $\bar{\boldsymbol{\varepsilon}}$ and $\mathbf{R}$ denote the transformed strain tensor and the transformation (also known as rotation) matrix, respectively. We rearrange equation 3 as

$$\mathbf{p} = \mathbf{G}\mathbf{m} \ , \tag{2}$$

where $\mathbf{p}$ and $\mathbf{m}$ are the transformed and original strain tensors respectively in vector form. The matrix $\mathbf{G}$ is the expansion of equation 3 using the transformation matrix $\mathbf{R}$ and contains all the geometric information about the optical fiber. For a single optical fiber, we have infinitely many strain projections along the optical fiber, where every projection being characterized by equation 2. To fully describe the DAS measurements $\mathbf{d}$, we use equation 2 and account for the axial strain averaging effect due to the gauge length as

$$\mathbf{d} = \mathbf{WAGm} \ , \tag{3}$$

where $\mathbf{A}$ is a convolution operator describing strain averaging within a gauge-length, and $\mathbf{W}$ is a windowing operator that defines the channel spacing which refers to the distance between consecutive average strain measurements within a gauge length. The graphical representation of equation 3 is

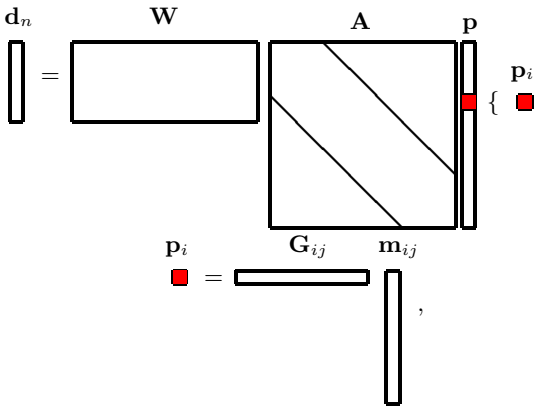

where indices i, j, and n represent samples along the optical fiber, components of the strain tensor, and measurements of a DAS system, respectively. Every sample i along the optical fiber is an element in the projection vector $\mathbf{p}$. Using the band matrix that describes the convolution operator $\mathbf{A}$, we capture the gauge length effect of the DAS system. In order to replicate a typical DAS system measurement, we apply a windowing operator $\mathbf{W}$ to determines the channel spacing between average strain measurements, usually equal to the gauge length. We represent the cascade operators of $\mathbf{WAG}$ as a linear operator $\mathbf{L}$. In the case when we obtain sufficient strain projections to describe the surrounding strain tensor, we can reconstruct the strain tensor $\mathbf{m}$ in a least-squares sense as

$$\mathbf{m} = (\mathbf{L^T L})^{-1}\mathbf{L^T d} \ . \tag{4}$$

To achieve accurate reconstruction using equation 4, the Gram matrix $\mathbf{L^T L}$ has to be invertible which is inferred from the

condition number associated with its singular values. Therefore, it is advantageous to use the condition number as an indicator of strain tensor reconstruction capabilities. This also provides us with an opportunity to access various optical fiber system designs, as discussed later.

Lim and Sava (2016) propose two configurations to obtain multiple strain projections to reconstruct the entire strain tensor. They demonstrate that two helical optical fibers of different constant pitch angles provide sufficient strain projections to accurately reconstruct the entire strain tensor. They also show that a single helical optical fiber with varying pitch angle is capable to provide adequate strain projections to reconstruct the entire strain tensor. In this reconstruction, Lim and Sava (2016) group n consecutive strain measurements (where $n \geqslant 6$ and possibly higher for improved SNR) along the optical fiber(s) within a defined window to obtain $\mathbf{d}$ in equation 4. Similarly, they group the associated linear operators $\mathbf{L}$ to form the Gram matrix. Although they demonstrate successful reconstruction, their approach has the drawback that it assumes a seismic wavelength significantly larger than the defined window for reconstruction. This drawback limits the application of this method to acquisition of long seismic wavelengths, thus reducing the resolution of seismic imaging with DAS data.

To overcome this drawback especially for applications that require short seismic wavelengths, we propose a configuration using six optical fibers to reconstruct all components of the strain tensor. Our approach is similar to the method of Lim and Sava (2016), as we use multiple strain projections to reconstruct the entire strain tensor using the formulation in equation 4. However, our configuration forms a full rank Gram matrix using measurements from individual optical fibers instead of spatially grouping consecutive measurements along a single optical fiber. Our new method allows us to reconstruct the strain tensor $\mathbf{m}$ in equation 4 at any given location using data $\mathbf{d}$ from individual measurements in the constituent optical fibers. The equivalent graphical representation of equation 3 for our proposed method

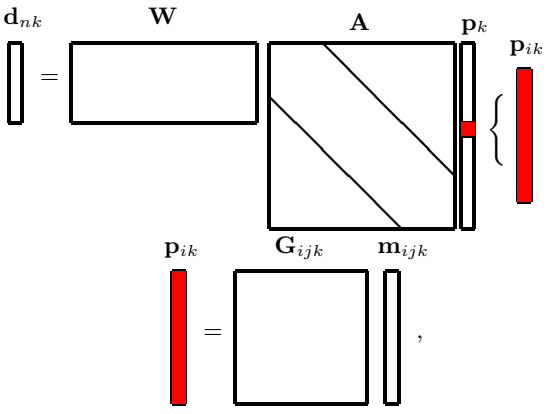

where index k denotes the number of optical fiber used for projections. Every sample i along the optical fiber k is given as an element in the projection vector $\mathbf{p}_k$. The presences of k optical fibers allow us to form the data vector $\mathbf{d}_{nk}$ and reconstruct the strain tensor $\mathbf{m}$ at a given location n. Note that the minimum requirement is to have $k = 6$ to reconstruct the six components of the strain tensor, which is similar to requirement of the method of Lim and Sava (2016) where they group $n \geqslant 6$ consecutive strain measurements.

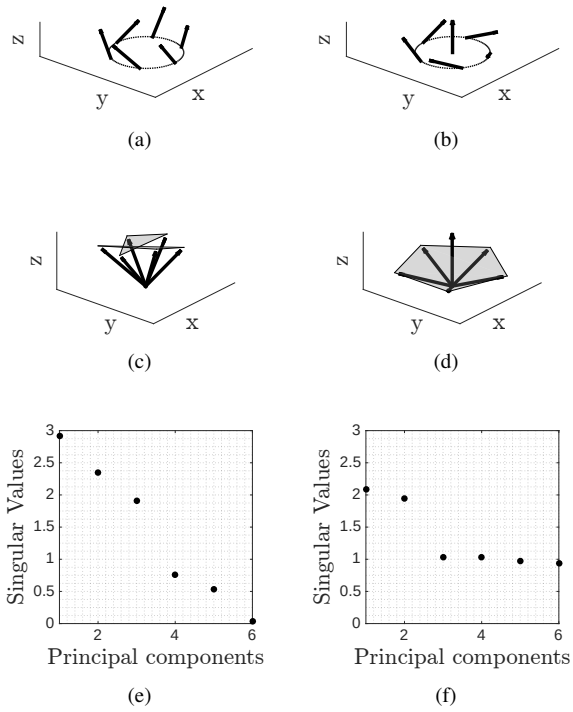

Figure 1. Optical fiber geometry with (a) **six** equally spaced vectors of six pitch angles (20°, 30°, 40°, 50°, 60°, and 70°), and (b) **five** equally spaced vectors of pitch angle of 20° with a straight vector in the middle. Panels (c) and (d) depict tetrahedra and right pentagonal pyramid respectively using the corresponding vectors in (a) and (b) sharing the same origin. The plots in (e) and (f) show singular values of the respective Gram matrices.

We represent individual optical fibers in our proposed configuration with tangent vectors to conceptually visualize the associated measurements as shown in Figure 1(a) with different pitch angles from 20° to 70° at every 10°. Figure 1(c) demonstrates that by using the same origin for all the vectors, we obtain a right pentagonal pyramid. The geometrical implication of our configuration provides insights on the associated strain projection, as discussed later. Using the projection matrix $\mathbf{G}$ of the individual vectors, we evaluate the singular values of $\mathbf{L^T L}$ as shown in Figure 1(e), which indicates that our configuration is full rank, despite the fact that the smallest singular value is close to zero. A full rank Gram matrix indicates that the corresponding configuration can reconstruct the entire strain tensor. However, using multiple helical optical fibers of different pitch angles increases the engineering complexity required to assemble the optical fiber system.

In order to simplify the design, we set our configuration to

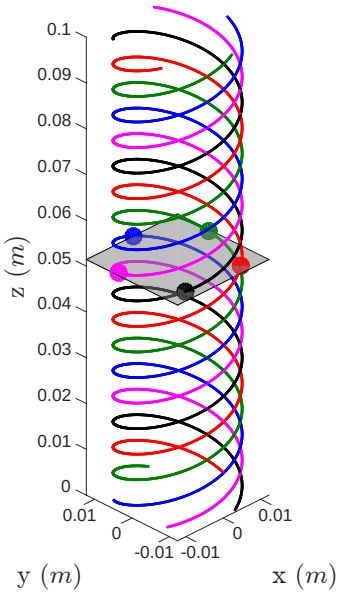

Figure 2. Example of five equally spaced helical optical fibers with a diameter of 1 in and a pitch angle of 20°. The dots represent measurement at the same length along respective fibers which refer to the same portion of the cable indicated by the horizontal plane. The straight vertical optical fiber is not included in this plot.

five equally spaced helical optical fiber with a 20° pitch angle, together with a straight optical fiber as shown in Figure 1(b). Rearranging the vectors to share the same origin allows us to form a right pentagonal pyramid, as shown in Figure 1(d). The straight fiber makes it possible to have all nonzero singular values, as seen in Figure 1(f), that infer a full rank Gram matrix. This configuration uses five equally spaced helical optical fibers with constant pitch angle is less manufacturing challenging than a sweeping helical optical fiber and allows us to obtain measurements at the same position in space along all the helical optical fibers (illustrated in Figure 2).

Using the configuration in Figure 1(b) and analyzing the condition number of the corresponding Gram matrix, we search for the optimum pitch angle between 5° to 50° as shown (solid line) in Figure 3. The lowest condition number is around 20°; at this angle the strain projections are mainly contributed by the horizontal components. The vertical vector in our arrangement provides only vertical strain projections. This implies that to accurately reconstruct the entire strain tensor; lower pitch angles are desirable to obtain projections from horizontal strain components as seen in Figure 3 where the condition number of the corresponding Gram matrix increases with the pitch angle from 20°. However, we avoid low pitch angles that are near horizontal to obtain projections from strain components between horizontal and vertical (i.e. ε_{xz} and ε_{yz}) for accurate reconstruction of the strain tensor as shown in Figure 3, where the condition number decreases as the pitch angle approaches 20°.

We investigate the effects of the geometrical change in Figure 1(d) associated with the pitch angle of our configuration in Figure 1(b) on the condition number of the corresponding Gram matrix. To quantitatively assess the geometrical implication of our configuration in Figure 1(d) which corresponds to a right pentagonal pyramid, we can calculate the surface-area-to-volume ratio (SA:V) as shown (dashed line) in Figure 3. SA:V provides us a measure of compactness of the geometry associated with our configuration. Figure 3 shows that the lowest SA:V (most compact geometry) corresponds to the pitch angle around 20°, which coincides with the lowest condition number of the Gram matrix associated with our configuration in Figure 1(b). Observing the geometry for high SA:V at 5° (Figure 4(a)) and 50° (Figure 4(c)), we can infer that the geometries that are flat or elongated do not provide a low condition numbers and thus do not lead to robust strain reconstruction. However, Figure 4(b) reveals a compact geometry with low SA:V that can provide sufficient projections to describe the surrounding strain tensor for full and accurate reconstruction.

We investigate the effects of the gauge length on the Gram matrix by considering single measurements as shown (dots) in Figure 2. The azimuthal variation of the five equally spaced optical fibers does not affect the Gram matrix as the spacing between measurements are invariant as a function of position along the optical fiber. Using the condition number of the Gram matrix, we can systematically obtain the optimum design parameters (gauge length, diameter and pitch angle of the helical optical fibers) associated with low condition numbers as shown in Figure 5 (the colors represent the logarithm of condition number). We can scan pitch angles from 15° to 35° and diameters of the helical optical cable from 0.01 to 0.03 m, for specific gauge lengths of 0.2, 0.4, 0.6, 0.8, and 1.0 m.

The strain measurement by the DAS system using a helical geometry undergoes strain averaging in the azimuthal direction along the optical fiber within a gauge length. When the gauge length is equal to a multiple of the helix lead (the axial advance of a helix for a complete 360° turn), the DAS measurement does not contain azimuthal information, which translates into an undeniable high condition number in Figure 5. If we increase the gauge length for the same diameter and pitch angle (fixed helical optical fiber design parameters), the condition number is increasingly oscillatory, as shown in Figure 5. The DAS measurement undergoes further azimuthal averaging within a longer gauge length, thus reducing the ability to accurately reconstruct the entire strain tensor. As we decrease the diameter of the helical optical fibers, the oscillations increase in frequency, which is also a result of increased azimuthal averaging. An informed reduction of the design parameters using the condition number ensures a high reconstruction accuracy.

In cases such as a borehole where dimensions (e.g. the diameter) are often limited, we can perform a two-dimensional parameter scan with one of the parameters fixed. In this paper, we show numerical examples of reconstructing the strain tensor using our new approach for identifying optimum parameters for a borehole environment, and we set the diameter of the optical fiber system at 1 in.

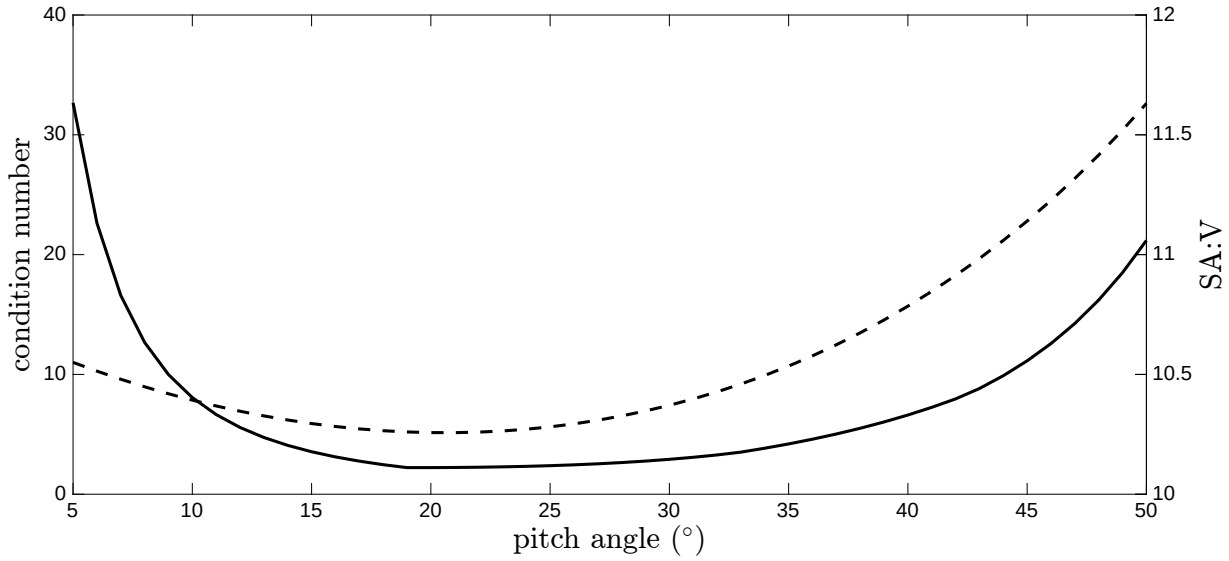

Figure 3. The solid line represents the condition number and the dashed line denotes the surface-area-to-volume ratio (SA:V) of a right pentagonal pyramid at different pitch angles for the five vectors in Figure 1(d). Both graphs share the same minimum at around 20° pitch angle.

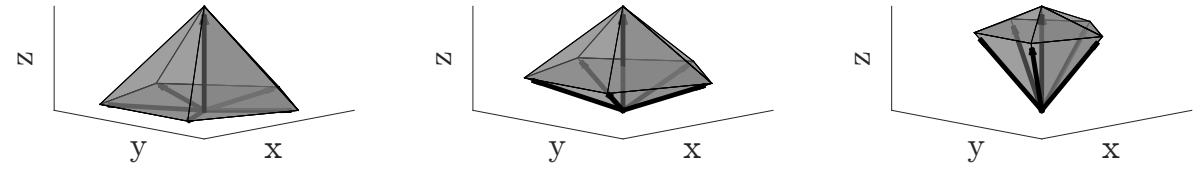

(a) (b) (c)

Figure 4. Two pentagonal pyramid using five vectors with pitch angles of (a) $\mathbf{5°}$, (b) $\mathbf{20°}$, and (c) $\mathbf{50°}$. The three pyramids show the visual relationship between the enclosed surface area and volume.

3 NUMERICAL EXAMPLES

Using numerical simulations, we reconstruct the entire 3D strain tensor with the parametrization analysis in a borehole scenario. In the following examples, we limit the dimensions of the helical optical fibers to a diameter of 1 in and a pitch angle of 20° as shown in Figure 2. By constraining the design parameters for the helical optical fibers, we can search for an optimum gauge length using the condition number of the Gram matrix as shown in Figure 6. In our example, we scan between 0.05 and 1.10 m; we observe that there are several local minima corresponding to low condition number throughout Figure 6. The corresponding gauge lengths at these local minima are optimal (i.e. higher accuracy) for strain tensor reconstruction. The oscillating characteristic of the condition number in Figure 6 shows that the gauge length has to be reduced systematically to ensure a low condition number for high reconstruction accuracy. We illustrate our following examples with gauge lengths of 0.1, 0.5, and 1.0 m, as shown (stars) in Figure 6. We choose the gauge length of 0.5 m that does not lie at a local minimum to demonstrate that the strain tensor reconstruct of a smaller gauge length may not necessary be superior to a larger gauge length. This phenomenon is shown through a similar level of reconstruction accuracy in Figure 9(c) (gauge length of 0.5 m) and Figure 9(e) (gauge length of 1.0 m).

Using synthetic examples of a complex wavefield, we illustrate the reconstruction of the three dimensional strain tensor from axial strain measurements along the proposed optical fiber geometry using different gauge lengths. We simulate using elastic finite-difference modeling a complex wavefield with triplications (Figure 7(d)) caused by a velocity model containing a low-velocity Gaussian anomaly, as shown in Figure 7(c). We use smaller than usual gauge lengths such as 0.1 and 0.5 m, which are possible using specially designed optical fibers, as indicated by Farhadiroushan et al. (2016). However, we also perform the analysis using a gauge length of 1.0 m to show the effect of a more conventional fiber system.

Our experiment setup with a source indicated by a dot and receivers indicated by a straight line of coordinates (x_b, y_b)

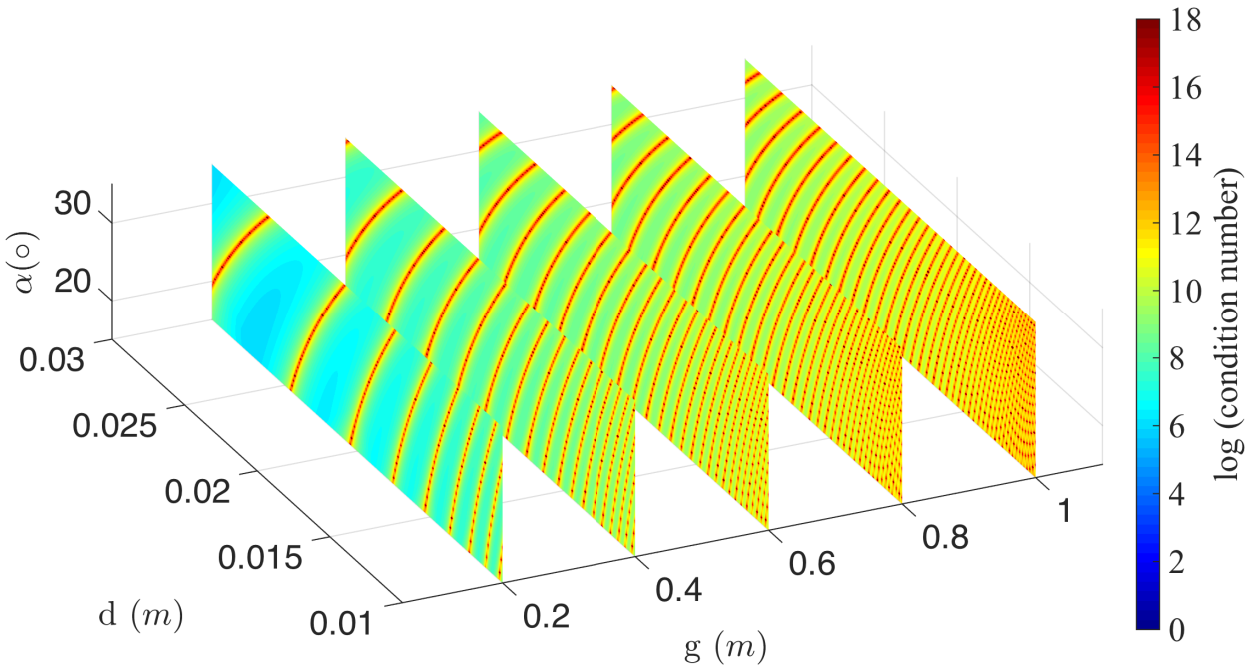

Figure 5. Condition number of the Gram matrix for pitch angle from 15° to 35° and diameter from 0.01 to 0.03 m. These slices are specifically scanned for but not limited to gauge lengths of 0.2, 0.4, 0.6, 0.8, and 1.0 m.

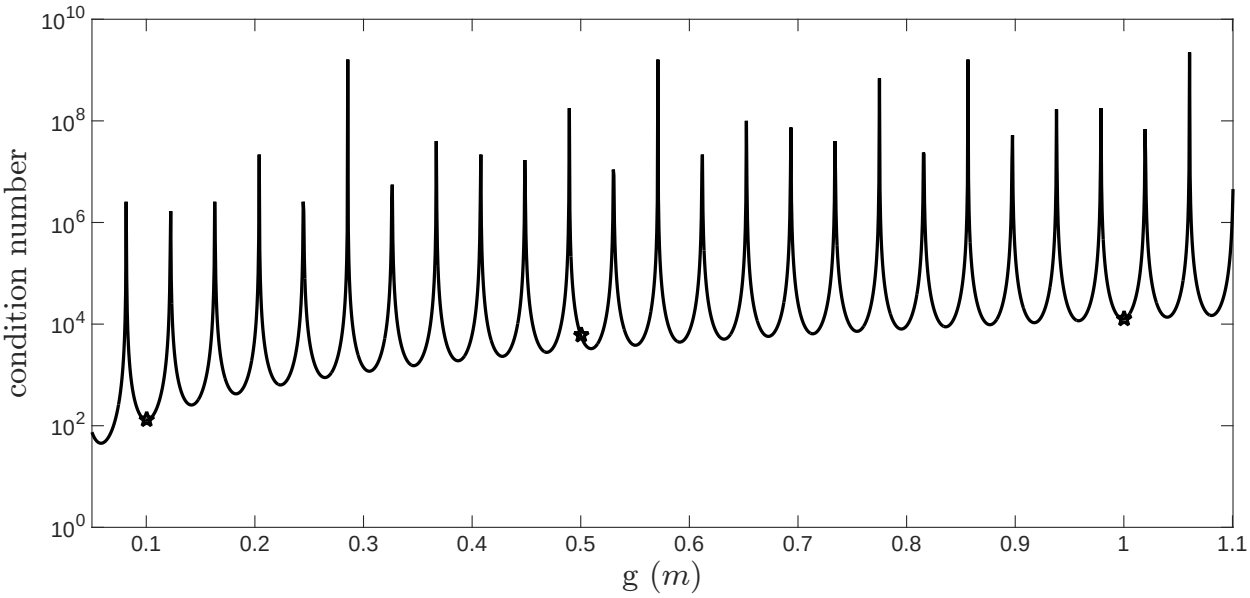

Figure 6. The plot shows a 1D parameter scan for the intersection between diameter of 1 in and 20° pitch angle of Figure 5. The stars mark the condition number for gauge lengths of 0.1, 0.5, and 1.0 m.

is shown in Figure 7(a). Figure 7(b), shown in a strain tensor matrix layout, represents our target strain tensor reconstruction observed along the receiver location at (x_b, y_b). The horizontal and vertical axes of the individual panels represent the reconstructed measurements along the optical fiber and time respectively. Using a gauge length of 0.1 m, we can reconstruct the strain tensor as shown in Figure 8(a). The difference plot between the observed and reconstructed strain tensor amplified 10 times is shown in Figure 8(b). We measure reconstruction quality with the residual sum of squares normalized as

$$\eta = \frac{\left\|\mathbf{m}^{obs} - \mathbf{m}^{rec}\right\|^2}{\left\|\mathbf{m}^{obs}\right\|^2} 100 \ , \tag{5}$$

where $\mathbf{m}^{obs}$ represents the observed strain tensor and $\mathbf{m}^{rec}$ represents the reconstructed strain tensor. The scalar values for η using a gauge length of 0.1 m are less than $10^{-4}\%$. Figure 8(c) shows the reconstructed strain tensor using the same configuration, but with the gauge length at 0.5 m. The differences in Figure 8(d) (also amplified 10 times) suggest that the increase of gauge length has minimal impact on our reconstruction. Although the calculated values for η increase overall with the larger gauge length, the highest η is less than $10^{-2}\%$, which is still a very high level of accuracy for practical applications. Figure 8(e) shows the results of performing the same reconstruction using a gauge length of 1.0 m. Although we can observe some minor differences in Figure 8(f) (also amplified 10 times), the highest η is less than $10^{-2}\%$ which is lower than the accuracy we get when we use a gauge length of 0.5 m. This result indicates that reducing the gauge length does not necessary improve the reconstruction accuracy; it moreover shows that careful analysis (as presented in Figure 6) of parameters is needed for accurate reconstruction.

Since the strain tensor reconstruction for the gauge lengths of 0.1, 0.5, and 1.0 m is successful without the presence of noise, we repeat the process by adding random noise with 30% of the maximum amplitude of the data (i.e. strain projections) and in the data frequency band. Using a gauge length of 0.1 m, the reconstruction shown in Figure 9(a) is a success. The difference plot in Figure 9(b) shows primarily random noise. Figure 9(c) shows the reconstruction results by increasing the gauge length to 0.5 m. We observe stronger arrivals although the results are noisy. The difference plot shown in Figure 9(d) contains noise primarily. Figure 9(e) shows the reconstruction using a gauge length of 1.0 m, and it shows a similar result compared to the gauge length of 0.5 m. The same observation applies to the difference plot in Figure 9(f). The comparable quality of reconstruction between gauge length of 0.5 and 1.0 m shows that reducing gauge length significantly (half in this case) does not guarantee improved reconstruction quality.

4 DISCUSSION

We demonstrate full strain tensor reconstruction with a high level of accuracy using six optical fibers (five equally spaced helical optical fiber with a pitch angle of 20° and a straight optical fiber). Our results under the presence of noise show the importance of design parameters using the condition number, as reducing the gauge length does not guarantee improvements in reconstruction. However, small but achievable gauge length with low condition number such as 0.1 m provides a robust strain tensor reconstruction due to the low condition number of the Gram matrix. A larger diameter of the helical configuration allows for a larger gauge length which improves the reconstruction results in noisier environments. A relaxed diameter dimension is more applicable in applications such as in a surface seismic acquisition.

Using our proposed configuration, we can analyze the design parameters for the helical optical fibers systematically. Scanning can be done in a general manner as shown in Figure 5 or under certain constraints (diameter or pitch angle of the helical optical fiber) as shown in Figure 6. The design goal is to obtain parameters that have the lowest possible condition number of the Gram matrix $\mathbf{G^T A^T A G}$ calculated from the averaging $\mathbf{A}$ and projection $\mathbf{G}$ matrices, while also satisfying engineering constraints for optical fiber construction. Numerous configuration of equivalent robustness and quality are possible. In the presence of optical fiber geometry uncertainty, we can use a weighting operator in the reconstruction process or the shape-sensing method (Moore and Rogge, 2012), as discussed in our previous paper (Lim and Sava, 2016) to improve our reconstruction results.

5 CONCLUSIONS

We demonstrate that high resolution multicomponent distributed acoustic sensing data is achievable by using strain projections along several optical fibers to reconstruct all components of the 3D strain tensor. Five equally spaced helical optical fibers, together with a straight optical fiber can be used for reconstruction without assuming that strain changes slowly along the fiber, as shown by Lim and Sava (2016). We thus overcome the requirement that the seismic wavelength be significantly larger than the window, and achieve multicomponent strain reconstruction with high spatial resolution. This method opens the possibility for acquisition of shorter seismic wavelengths, which aids imaging and reservoir characterization applications. Numerical examples show that our method can reconstruct the full 3D strain tensor for wavefields of arbitrary complexity, and in the presence of strong noise in the band of the seismic data.

6 ACKNOWLEDGMENTS

We would like to thank the sponsors of the Center for Wave Phenomena, whose support made this research possible and Martin Karrenbach of OptaSense for fruitful discussions. The reproducible numeric examples in this paper use the Madagascar open-source software package (Fomel et al., 2013) freely available from http://www.ahay.org.

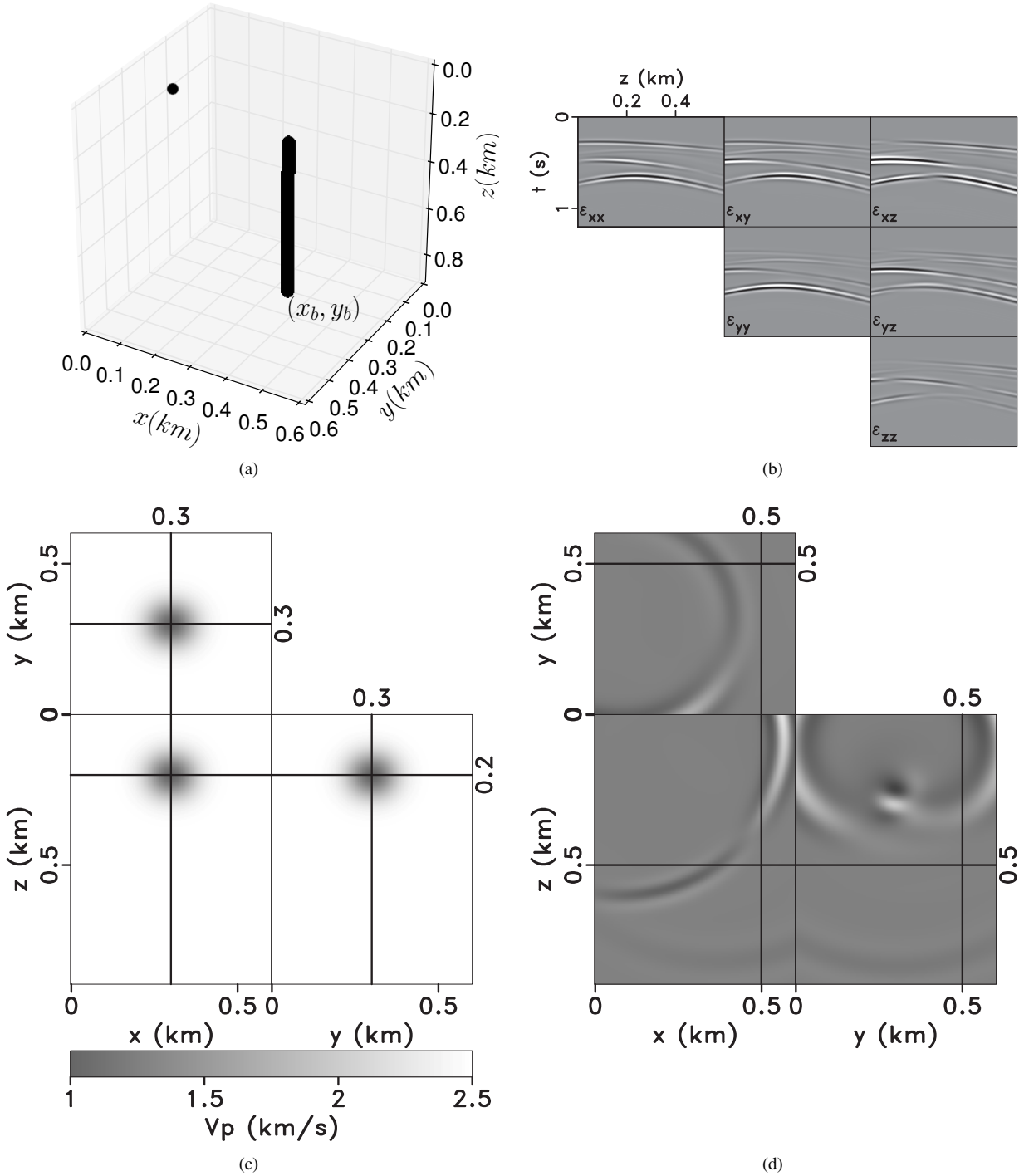

Figure 7. (a) Schematic representation of a DAS experiment depicting the source (dot) and receiver (line) locations. (b) The ideal strain tensor that we would like to reconstruct from DAS measurements. (c) The P-wave velocity model containing a low velocity Gaussian anomaly designed to produce wavefield triplications. The S-wave velocity is half of the P-wave velocity. (d) A snapshot of the vertical displacement wavefield.

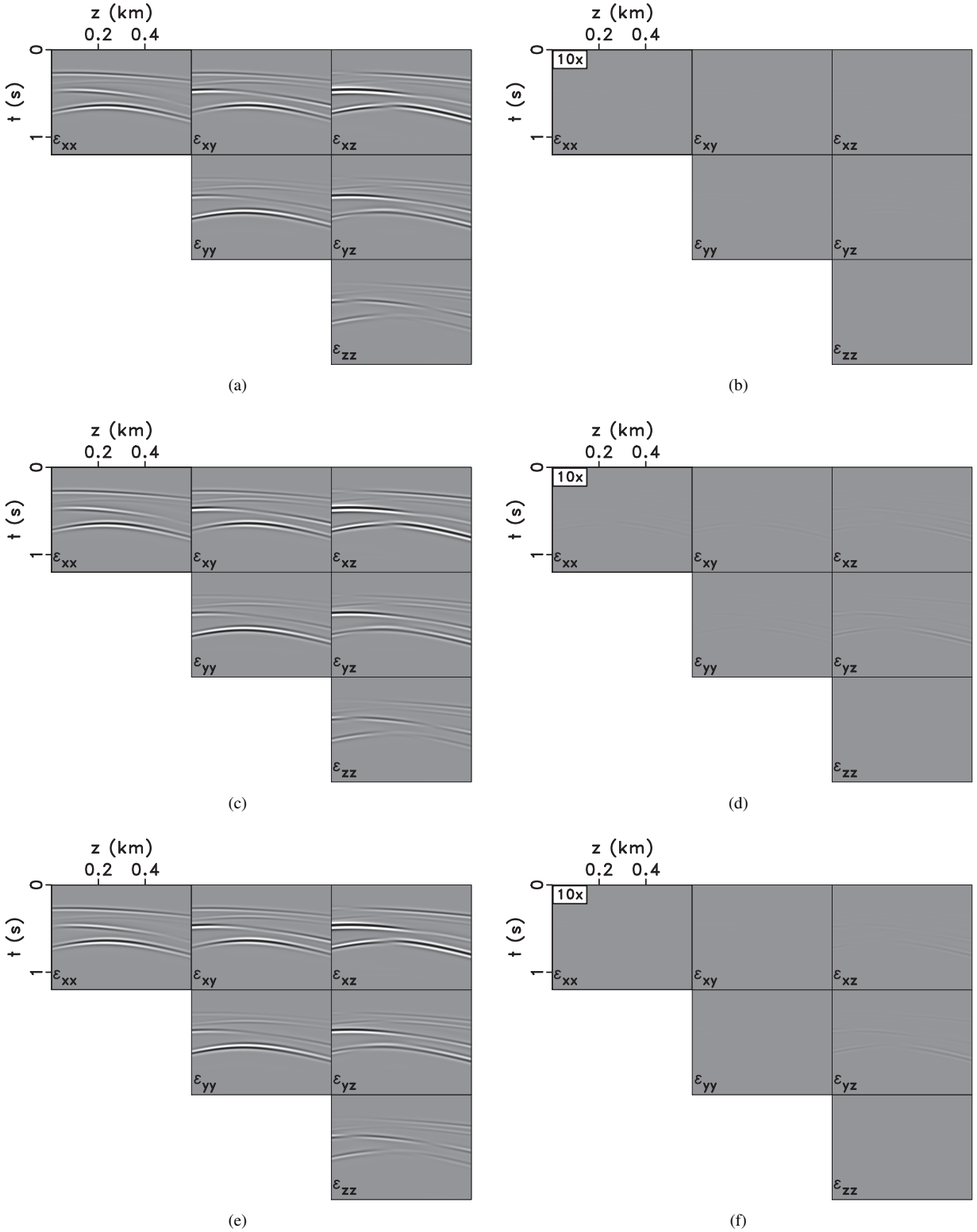

Figure 8. Strain tensor reconstructed with five equally spaced helical optical fibers and a straight optical fiber using a gauge length of (a) 0.1 m, (c) 0.5 m, and (e)1.0 m. (b), (d), and (f) are the difference between the ideal strain tensor in Figure 7(b) and the respective reconstructed tensor in (a), (c), and (e) magnified 10 times.

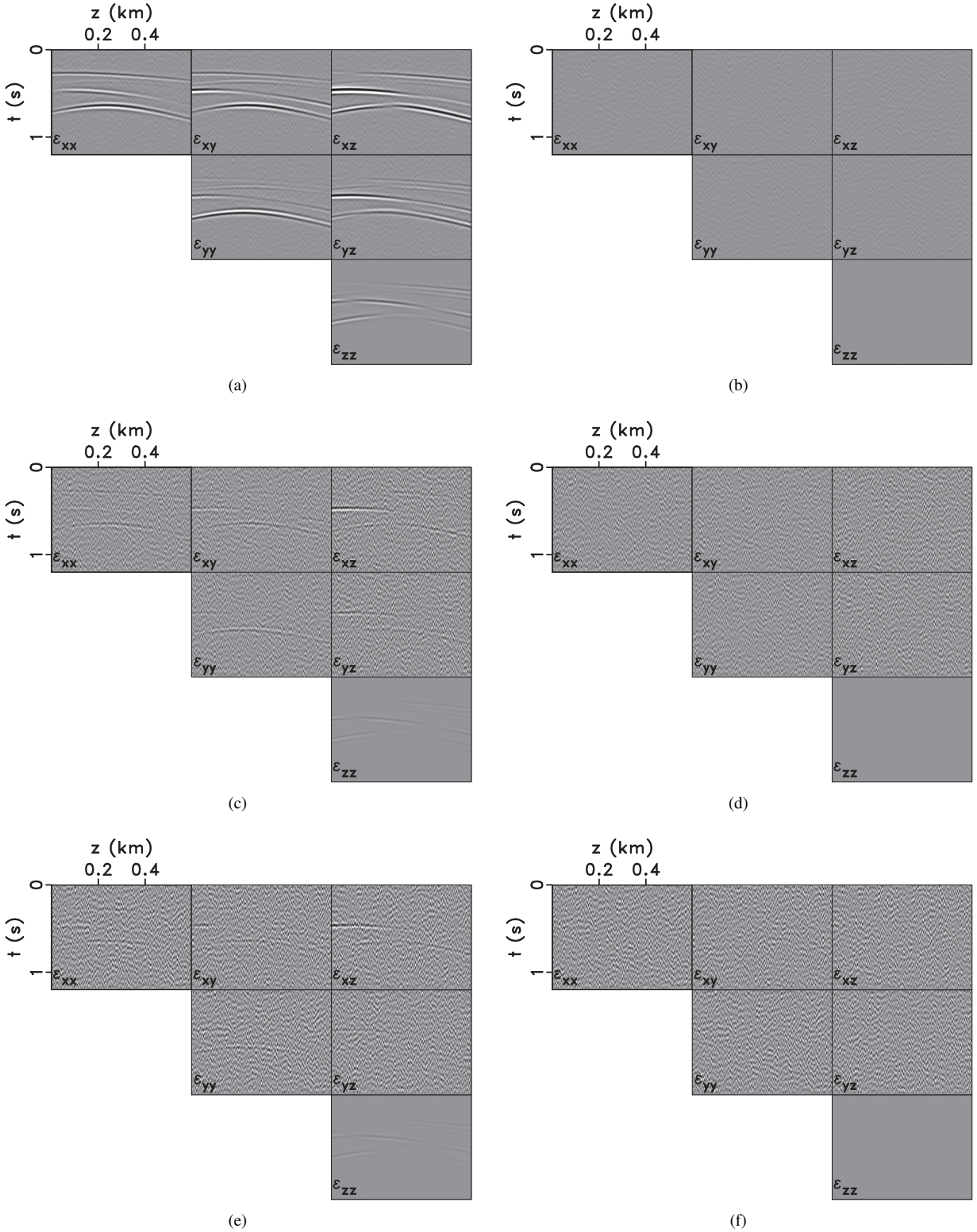

Figure 9. Strain tensor reconstructed from data containing random noise with 30% of the maximum data amplitude and band-limited to the data band with five equally spaced helical optical fibers and a straight optical fiber using a gauge length of (a) 0.1 m, (c) 0.5 m, and (e) 1.0 m. (b), (d), and (f) are the difference between the ideal strain tensor in Figure 7(b) and the respective reconstructed tensor in (a), (c) and (e).

REFERENCES

Bakku, S. K., 2015, Fracture characterization from seismic measurements in a borehole: PhD thesis, Massachusetts Institute of Technology.

Chalenski, D., M. Tatanova, Y. Du, A. Mateeva, J. Lopez, and H. Potters, 2016, Climbing the staircase of ultralow-cost 4D monitoring of deepwater fields using DAS-VSP, *in* SEG Technical Program Expanded Abstracts 2016: Society of Exploration Geophysicists, 5441–5445.

Dou, S., J. Ajo-Franklin, T. Daley, M. Robertson, T. Wood, B. Freifeld, R. Pevzner, J. Correa, K. Tertyshnikov, M. Urosevic, et al., 2016, Surface orbital vibrator (SOV) and fiber-optic DAS: Field demonstration of economical, continuous-land seismic time-lapse monitoring from the australian CO2CRC Otway site, *in* SEG Technical Program Expanded Abstracts 2016: Society of Exploration Geophysicists, 5552–5556.

Farhadiroushan, M., T. Parker, and S. Shatalin, 2016, Method and apparatus for optical sensing. (WO Patent App. PCT/GB2016/050,625).

Fomel, S., P. Sava, I. Vlad, Y. Liu, and V. Bashkardin, 2013, Madagascar: open-source software project for multidimensional data analysis and reproducible computational experiments: Journal of Open Research Software, **1**.

Hornman, J., A. Mateeva, J. Potters, and J. Lopez, 2015, New concepts for lowering the cost of frequent seismic reservoir monitoring onshore, *in* SEG Technical Program Expanded Abstracts 2015: Society of Exploration Geophysicists, 5518–5522.

Jiang, T., G. Zhan, T. Hance, S. Sugianto, S. Soulas, and E. Kjos, 2016, Valhall dual-well 3D DAS VSP field trial and imaging for active wells, *in* SEG Technical Program Expanded Abstracts 2016: Society of Exploration Geophysicists, 5582–5586.

Li, Y., H. Wu, W. Wong, B. Hewett, Z. Liu, A. Mateeva, and J. Lopez, 2015, Velocity analysis and update with 3D DAS-VSP to improve borehole/surface seismic images, *in* SEG Technical Program Expanded Abstracts 2015: Society of Exploration Geophysicists, 5285–5289.

Lim, I. C. N., and P. Sava, 2016, Multicomponent distributed acoustic sensing, *in* SEG Technical Program Expanded Abstracts 2016: Society of Exploration Geophysicists, 5597–5602.

Lumens, P. G. E., 2014, Fibre-optic sensing for application in oil and gas wells: PhD thesis, Technische Universiteit Eindhoven.

Mateeva, A., J. Lopez, J. Mestayer, P. Wills, B. Cox, D. Kiyashchenko, Z. Yang, W. Berlang, R. Detomo, and S. Grandi, 2013, Distributed acoustic sensing for reservoir monitoring with VSP: The Leading Edge, **32**, 1278–1283.

Mateeva, A., J. Mestayer, B. Cox, D. Kiyashchenko, P. Wills, J. Lopez, S. Grandi, K. Hornman, P. Lumens, A. Franzen, et al., 2012, Advances in distributed acoustic sensing (DAS) for VSP: Presented at the 2012 SEG Annual Meeting, Society of Exploration Geophysicists.

Mestayer, J., B. Cox, P. Wills, D. Kiyashchenko, J. Lopez, M. Costello, S. Bourne, G. Ugueto, R. Lupton, G. Solano, et al., 2011, Field trials of distributed acoustic sensing for geophysical monitoring: Presented at the 2011 SEG Annual Meeting, Society of Exploration Geophysicists.

Moore, J. P., and M. D. Rogge, 2012, Shape sensing using multi-core fiber optic cable and parametric curve solutions: Optics express, **20**, 2967–2973.

Pisano, A. P., 1988, The differential geometry of the general helix as applied to mechanical springs: Journal of Applied Mechanics, **55**, 831.

Wu, H., W.-F. Wong, Z. Yang, P. B. Wills, J. L. Lopez, Y. Li, B. Blonk, B. Hewett, and A. Mateeva, 2015, Dual-well 3D vertical seismic profile enabled by distributed acoustic sensing in deepwater Gulf of Mexico: Interpretation, **3**, SW11–SW25.

Young, W. C., and R. G. Budynas, 2002, Roark's formulas for stress and strain: McGraw-Hill New York, **7**.

Zhan, G., J. Kommedal, and J. Nahm, 2015, VSP field trials of distributed acoustic sensing in Trinidad and Gulf of Mexico, *in* SEG Technical Program Expanded Abstracts 2015: Society of Exploration Geophysicists, 5539–5543.